Nanoscale

RSC Publishing

PAPER

View Article Online
View Journal | View Issue

Cite this: *Nanoscale*, 2013, 5, 422

Programmable complementary resistive switching behaviours of a plasma-oxidised titanium oxide nanolayer

Guangsheng Tang, Fei Zeng,* Chao Chen, Hongyan Liu, Shuang Gao, Cheng Song, Yisong Lin, Guang Chen and Feng Pan*

Received 13th September 2012
Accepted 7th November 2012

DOI: 10.1039/c2nr32743k

www.rsc.org/nanoscale

Through the one-step plasma oxidation of TiN thin films at room temperature (a simple semiconductor technology compatible method), a partly oxidised structure of titanium oxynitride (TiN_xO_y) with a TiO_{2-x} nanolayer on top has been prepared for non-volatile resistive switching memory devices. The fabricated $Pt/TiO_{2-x}/TiN_xO_y/TiN$ memory devices demonstrate complementary resistive switching behaviours within an operation voltage of 1 V. The complementary resistive switching behaviours can be explained by redistribution of the oxygen vacancies between the Pt/TiO_{2-x} top interface and the TiO_{2-x}/TiN_xO_y bottom interface in the TiO_{2-x} nanolayer. A model concerning the resistive switching mechanism as well as a recover program of a failed device is also proposed. Our work provides a possible cost-efficient solution to suppress the sneak-path problem in nanoscale crossbar memory arrays.

Introduction

Resistive-switching random access memory (RRAM) is attracting increasing attention as one of the most promising candidates for next-generation nonvolatile memory (NVM) due to its simple structure, high scalability and high switching speed.[1] The simplicity of the metal–insulator–metal (MIM) structure enables RRAM to be integrated in passive crossbar arrays, and the memory cell size can be reduced to $4F^2/n$ (F is the minimum feature size; n is the stacking layer number of the crossbar arrays).[2] However, the operation of a specific cell is easily disturbed by the so-called crosstalk problem resulting from unintended multiple parallel sneak paths in the crossbar network. Furthermore, a greater power consumption is required for the crossbar arrays if the memory cells are mainly in the low resistance state (LRS). Several selection elements are proposed to suppress the crosstalk, such as adding a threshold switch, a PN junction diode or a Schottky diode for the unipolar RRAM.[3] An intrinsic rectifying structure was proposed for silicon-based bipolar RRAM;[4] while a threshold switch or a symmetric nonlinear resistor was used for metal oxide-based bipolar RRAM with some progress.[5] Recently, a concept of complementary resistive switches (CRS) has been suggested to solve the crosstalk problem by connecting two bipolar RRAM cells antiserially.[6] A typical CRS shows a superimposed current–voltage (I–V) characteristic of the two merged memory cells, and switches between '1' and '0' by setting one of the cells in the LRS and the other in the high resistance state (HRS) alternately. Thus, both the crosstalk and the large power consumption fluctuation of the crossbar arrays problems could be overcome without adding another element. Among these solutions, the advantage of CRS is that its principle can be used with any bipolar RRAMs.[6] This concept was soon applied to an asymmetric Ta_2O_{5-x}/TaO_{2-x} bilayer CRS, which demonstrates a successful crossbar device.[7] Then, homo $TiO_x/TiO_y/TiO_x$ and hetero $TiO_x/TiON/TiO_x$ triple multilayer structures without the additional middle Pt electrode were proposed for CRS construction.[8] Furthermore, Yang *et al.* reported complementary resistive switching behaviours in a simpler Ta_2O_{5-x}/TaO_y bilayer cell due to oxygen vacancies exchanging between two layers.[9] Though the above processes have been made, potential issues for scientific and technical interests remain to be considered, such as the understanding of the dynamic process of CRS, the development of CRS in a single nanolayer based RRAM to further simplify the memory structure and fabrication process, reducing the operation voltage (<1 V) compatible for mobile storage,[10] and so on.

Herein, we demonstrate programmable complementary resistive switching behaviours in a TiO_{2-x} nanolayer-based RRAM within an operation voltage of 1 V, revealing that complementary switching can be realised in a single metal oxide layer.[11] Titanium oxide was selected as the storage medium in this work for two reasons. First, titanium is much more abundant in the earth as compared with its memory competitors, such as tantalum and hafnium, guaranteeing a low-cost application. Second, titanium oxide can be fabricated by the one-step plasma oxidation of TiN thin films at room

Key Laboratory of Advanced Materials (MOE), Department of Materials Science and Engineering, Tsinghua University, Beijing 100084, P.R. China. E-mail: zengfei@mail.tsinghua.edu.cn; panf@mail.tsinghua.edu.cn; Fax: +86-10-62771160; Tel: +86-10-62795373

temperature. Plasma oxidation, which is thought to be very convenient for the accurate control of thickness and layer resistance, is becoming a low-cost and powerful tool to fabricate RRAM devices.[7,12] Also, this process is completely compatible with standard semiconductor technology. We proposed a dynamic process to understand the resistive switching (RS) mechanisms, which can guide us in the development of cost-efficient nanoscale CRS devices.

Experimental

TiN thin films were grown on SiO_2/Si substrates by direct current reactive magnetron sputtering with a titanium target, and the working gas was a mixture of argon (0.15 Pa) and nitrogen (0.25 Pa). The subsequent plasma oxidation was performed with a home-built radio frequency (RF) plasma system for 5 min. The oxidation process was conducted with a RF power of 300 W, board voltage of 1200 V and a working pressure of 40 Pa with a pure O_2 flow rate of 40 SCCM (SCCM denotes cubic centimetre per minute at standard temperature and pressure) at room temperature. Circular Pt top electrodes (TE) with a diameter of 300 μm were fabricated by magnetron sputtering using a metal shadow mask. The thickness of Pt TE, plasma oxidised layer and TiN bottom electrode (BE) was about 150, 30 and 100 nm, respectively. The resistive switching behaviours of the memory devices were measured using an Agilent B1500A semiconductor parameter analyser in the voltage sweeping model at room temperature. During the measurements, bias voltages were applied on the Pt TE with the TiN BE grounded. The microstructure of the plasma oxidised films was characterized by transmission electron microscopy (TEM, JEOL-2010F) with a field emission e-beam gun, and the chemical states were analysed by X-ray photoelectron spectroscopy (XPS, Escalab 250Xi) with Al Kα radiation of 1486.6 eV. Temperature-dependent resistance was measured at <0.1 V on a physical property measurement system (PPMS, Quantum Design).

Results and discussion

A cross-sectional TEM image of the plasma oxidised layer can be examined in Fig. 1A. One can clearly see a 30 nm thick oxidised layer with bright contrast, and a thin layer (~4 nm) with darker contrast near the surface, revealing a partly oxidised (*e.g.*, TiN_xO_y) layer with a highly oxidised nanolayer (*e.g.*, TiO_{2-x}) on top. Fig. 1B further illustrates a high-resolution TEM image at the interface between the oxidised layer and the TiN BE, which apparently shows an amorphous structure of the plasma oxidised layer. The amorphous structure could be attributed to the effect of the collision cascade of atoms by oxygen ion bombardment during the plasma oxidation process, which could be commonly observed on the surface of various materials by low energy ion beam bombardment.[13] In order to determine the chemical state of the plasma oxidised layer, Ti 2p core-level XPS spectra were investigated. These spectra were measured on the as-prepared surface and after Ar^+ ion beam sputtering with an energy of 1 keV and an estimated etching speed of ~0.06 nm s^{-1}. The XPS spectrum of the as-prepared

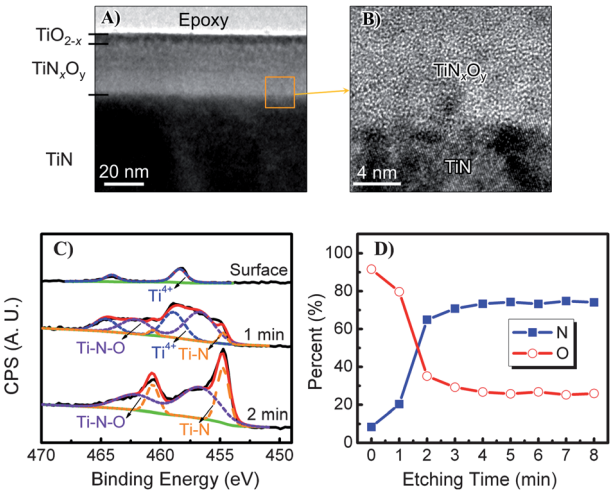

Fig. 1 (A) Cross-sectional TEM image of the plasma oxidised TiN thin film. (B) High-resolution TEM image of the interface between the plasma oxidised layer and the TiN BE. (C) XPS core-level spectra and fitting results of Ti 2p taken at the surface and after sputtering with Ar^+ for 1 and 2 min, respectively. (D) Relative content of N and O *versus* etching time determined by XPS depth profile analysis.

surface exhibits two peaks of Ti $2p_{3/2}$ at 458.4 eV and Ti $2p_{1/2}$ at 464.1 eV (Fig. 1C). The value was close to the reported data of TiO_2, where Ti $2p_{3/2}$ was located at 458.7 eV and Ti $2p_{1/2}$ at 464.4 eV,[14] while the shift of the spectra suggests a non-stoichiometric defective TiO_{2-x} layer on the surface. After sputtered by the Ar^+ ion beam, the Ti 2p spectra became broader and new peaks appeared at 456.7 and 454.7 eV, indicating the presence of Ti–N–O and Ti–N bonds, respectively.[15] The TiO_2 peak content decreased with the increase of etching time and disappeared after sputtering for 2 min, while the peak content of Ti–N–O and Ti–N bonds increased. Furthermore, the nitrogen and oxygen relative content *versus* etching time was also investigated by XPS semi-quantitative analysis (Fig. 1D). Clearly, a sharp oxygen content drop is observed within the first 2 minutes of sputtering and the decrease becomes gentle with increasing etching time, suggesting a thin TiO_{2-x} nanolayer with a thickness of about 4 nm was formed on the surface, which agrees well with the TEM observation (Fig. 1A). The beneath oxidised layer is regarded as titanium oxynitride (TiN_xO_y) with low oxygen content ($x/y > 3$), which is proposed to be conductive.[16] Hence, the initial TiO_{2-x} nanolayer may act as an insulator for a resistive switching application, while the TiN_xO_y layer may act as an oxygen reservoir, as discussed below.

A schematic configuration of the Pt/TiO_{2-x}/TiN_xO_y/TiN device and the *I–V* setup is depicted in Fig. 2A. Typical *I–V* curves of the devices for consecutive 50 cycles are shown in Fig. 2B, demonstrating well-defined clockwise (CW) bipolar RS with a high degree of repeatability. The as-prepared devices exhibit a high resistance of ~10^6 Ω. A low electroforming voltage (~−2 V) is required for the Pt/TiO_{2-x}/TiN_xO_y/TiN devices, which could be attributed to the amount of defects, such as oxygen vacancies, pre-existing in the as-prepared TiO_{2-x} layer during plasma oxidation. An applied voltage was swept in a sequence of 0 V → 1.5 V → 0 V → −1.5 V → 0 V on the device. By steadily increasing the positive voltages, a resistance change from LRS

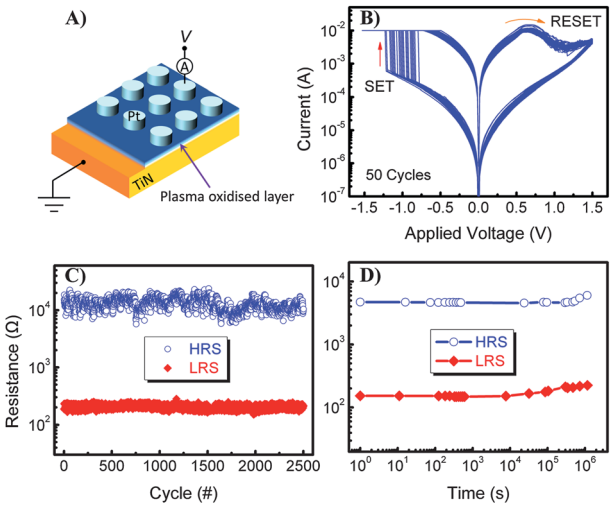

Fig. 2 (A) A schematic configuration of the three-dimensional Pt/TiO_{2-x}/TiN_xO_y/TiN device. (B) *I–V* curves of a Pt/TiO_{2-x}/TiN_xO_y/TiN device for 50 consecutive switching cycles on the semi-logarithmic scale. (C) Endurance performance and (D) retention of the devices. The resistance was read out at 0.1 V.

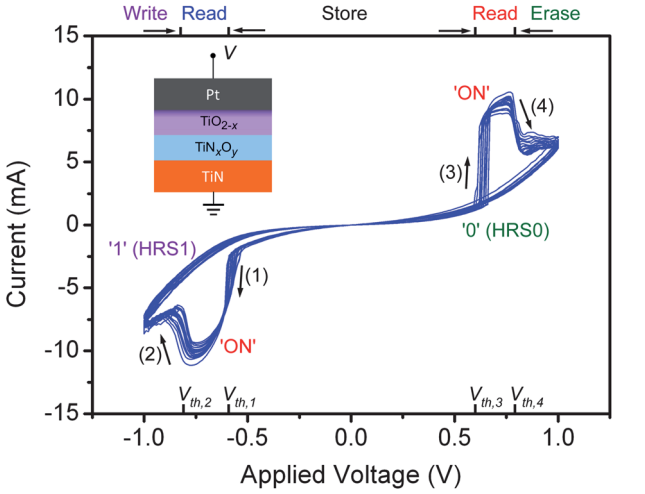

Fig. 3 *I–V* curves of the Pt/TiO_{2-x}/TiN_xO_y/TiN device demonstrating complementary resistive switching behaviours when a voltage is swept in the range of (−1, 1) V. The blue curves represent 20 consecutive cycles, which show a high degree of repeatability. The four-switching process is marked as (1–4). Inset: a schematic cross-sectional structure of the device.

to HRS was observed beyond ~0.7 V, which is called the RESET process. Subsequently, as the applied voltage swept from zero to negative voltages, an opposite SET process could also be seen at −0.8 to −1.2 V. The RS behaviours are in agreement with the previously reported Pt/TiO_2/TiN system RRAM devices.[17] The endurance and retention characteristics of the Pt/TiO_{2-x}/TiN_xO_y/TiN devices were also investigated. As displayed in Fig. 2C, the device shows an endurance of >2500 cycles with little degradation. Besides, no significant changes in the resistance magnitudes for more than 10^6 s could be observed at room temperature, as shown in Fig. 2D. The excellent endurance and retention properties of the Pt/TiO_{2-x}/TiN_xO_y/TiN devices ensure their potential application in the RRAM industry.

More interestingly, complementary resistive switching behaviours can also be demonstrated in the Pt/TiO_{2-x}/TiN_xO_y/TiN device through proper programming. After an electroforming process under a negative bias (~−2 V), the initial (as-prepared, in HRS) device was switched to the electroformed state in LRS. Then the device was switched to a HRS (denoted as HRS0) by applying a 'soft' RESET process (1 V), as compared to a 'hard' RESET process at large voltage (*e.g.*, 1.5 V). Subsequently, when the applied voltage *V* was swept in a sequence of 0 V → −1 V → 0 V → 1 V → 0 V, the devices demonstrated four-switching process behaviours with high repeatability as denoted as (1–4) in Fig. 3: (1) with the applied voltage increasing under a negative bias, a current jump took place at a threshold voltage (~0.6 V, denoted as $V_{th,1}$), and then the device was turned into the LRS (denoted as 'ON' state). (2) Further increasing the negative voltage, caused a current drop to occur at another threshold voltage (~−0.8 V, denoted as $V_{th,2}$), afterwards, the device was switched to another HRS (denoted as HRS1). (3) As the applied voltage reached a positive threshold voltage (~0.6 V, denoted as $V_{th,3}$), the device was switched from HRS1 to LRS ('ON' state), which was kept until reaching a larger positive threshold (~0.8 V, denoted as $V_{th,4}$). HRS1 was maintained in the voltage range of (−1 V, $V_{th,3}$). (4) The device was returned to HRS0 again when $V > V_{th,4}$, which was maintained in the voltage range of ($V_{th,1}$, 1 V). Hence, HRS0 and HRS1 can be regarded as the '0' and '1' states of the device, respectively, which can be distinguished by the application of a read voltage *V* into the range $V_{th,3} < V < V_{th,4}$ (*e.g.*, the region marked with 'Read' in red colour in Fig. 3). In this case, HRS0 is kept in the HRS, while HRS1 is switched to the LRS ('ON' state). The erase operation (turn to '0') can be realised by application of a voltage $V > V_{th,4}$, and the write operation (turn to '1') by application of a voltage $V < V_{th,2}$ (*e.g.*, the region marked with 'Erase' and 'Write' in Fig. 3, respectively). On the contrary, if HRS0 and HRS1 is defined as the '1' and '0' states of the device, respectively, then the read voltage should satisfy $V_{th,1} < V < V_{th,2}$, with an erase voltage $V < V_{th,2}$ and a write voltage $V > V_{th,4}$. The symmetrical *I–V* curves, as shown in Fig. 3, could be attributed to that ohmic-like contact that was formed not only at the TiO_{2-x}/TiN_xO_y interface,[18] but also at the Pt/TiO_{2-x} interface, because the resistance of the HRS was several kilo-ohms due to the oxygen deficiency in the TiO_{2-x} layer.[1a,19] The four-switching process behaviours are analogous to that reported in anti-serially stacked CRSs.[6] Because both '0' and '1' stored in the CRS cells are in the HRS at low bias (*e.g.*, $V_{th,1} < V < V_{th,3}$, the region marked with 'Store' in Fig. 3), the device ensures the capability of suppressing the crosstalk and large power consumption fluctuation problems in the crossbar arrays.

For the RRAM based on oxides sandwiched by two inert electrodes, the reversible resistive switching is commonly attributed to oxygen vacancies (ions).[1a,8,20] Previous studies of titanium oxide RRAMs have shown that the bipolar resistive switching can be well modelled with a tunnelling barrier or other non-linear transport barrier.[1a,20b,21] The electronic conduction in the devices with such a barrier can be modulated by applying a voltage across the device and inducing the motion of ionized defects, such as oxygen vacancies.[21a] Oxygen

vacancies can be formed during electroforming as described in Kröger–Vink notation *via* eqn (1):

$$O_o \rightarrow \frac{1}{2}O_2(g) + V_o^{\bullet\bullet} + 2e^- \quad (1)$$

where O_o and $V_o^{\bullet\bullet}$ denote oxygen ions on regular lattice sites and oxygen vacancies, respectively.[1c] Once the electroforming is completed, bipolar RS is possible under a reverse bias.

To clarify the switching mechanism of our devices, we measured the temperature-dependent resistance for the LRS and HRS at low voltage (<0.1 V) with temperatures varying between 300 and 80 K. As shown in Fig. 4A, the resistance of the LRS, including both the electroformed state and the 'ON' state, show an increasing trend with decreasing temperature, indicating that the conduction is not metallic but semiconducting. The temperature-dependent resistance of the HRS also shows a typical semiconducting behaviour (Fig. 4B). Furthermore, the thermal activation energy Φ_t was calculated *via* the relationship $R = R_0\exp(\Phi_t/kT)$ (k is the Boltzmann constant, T is the temperature).[22] The thermal activation energy of the HRS is ~38 meV at room temperature, which agrees with the reported activation energy of TiO_{2-x} in the equivalent resistance level.[23] The HRS–LRS change should be due to the variation of the tunnel barrier, which can be modulated by oxygen vacancy defects.[1a,b,21a] The barrier of the LRS is lower than that of the HRS because it is rich in oxygen vacancies.

With the above analysis, the RS processes can be explained by taking into account the oxygen vacancy migration under a bias voltage and the contributions of both the Pt/TiO_{2-x} top and TiO_{2-x}/TiN_xO_y bottom interfaces. Here, the TiO_{2-x} nanolayer is assumed to consist of two resistor regions in a series: one at the Pt/TiO_{2-x} top interface (R_{top}) and the other at the TiO_{2-x}/TiN_xO_y bottom interface (R_{bot}), as shown in Fig. 5A. The TiN_xO_y layer is always supposed to be in the LRS and more importantly plays an essential role in modulating the oxygen vacancy concentration in the TiO_{2-x}/TiN_xO_y bottom interface. Fig. 5A shows the initial state of the memory cell with both the Pt/TiO_{2-x} top and TiO_{2-x}/TiN_xO_y bottom interfaces in the HRS (R_{top}/R_{bot} in HRS/HRS). Under a negative bias voltage, a large number of oxygen vacancies are introduced in the TiO_{2-x} nanolayer by electroforming so that an oxygen-deficient conductive channel penetrates both regions and allows them to be switched to the LRS (R_{top}/R_{bot} in LRS/LRS, as shown in Fig. 5B). Simultaneously, the as-formed oxygen atoms *via* eqn (1) can be 'stored' in the TiN_xO_y layer (acting as an oxygen reservoir) through an oxidation or/and a physical adsorption process, also implying the ability to solve the oxygen gas evolution problem.[24] When applying a large positive voltage (*e.g.*, hard RESET at 1.5 V), the oxygen vacancies drift towards the BE and the oxygen vacancy concentration in the top interface decreases so that R_{top} is switched to the HRS; besides, annihilation of the oxygen vacancies can occur in the TiN_xO_y layer (acting as an oxygen provider in this case) through a reduction process, so that R_{bot} is also switched to the HRS (Fig. 5C). Consequently, R_{top}/R_{bot} can be switched between the HRS/HRS and LRS/LRS by the application of an alternative bias voltage, demonstrating conventional bipolar RS behaviours, as shown in Fig. 2.

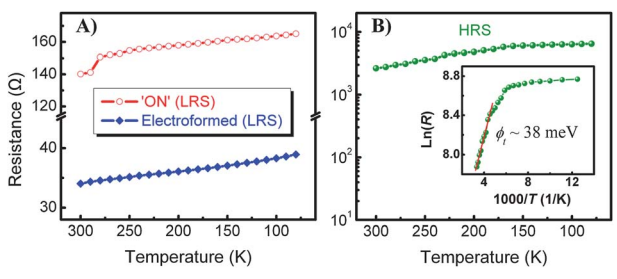

Fig. 4 Temperature-dependent resistance of a Pt/TiO_{2-x}/TiN_xO_y/TiN device measured between 80 and 300 K: (A) *R–T* curves of the device in the electroformed state and 'ON' state (LRS); (B) *R–T* curve of the device in the HRS, the inset is the corresponding Arrhenius plots. All these states of the device imply semiconducting behaviours.

We now turn towards the mechanism for the complementary resistive switching of our devices. As shown in Fig. 5D, when applying a proper positive voltage (*e.g.*, soft RESET at 1 V), a large amount of oxygen vacancies drift from the top interface region into the bottom interface region so that R_{top} is switched to the HRS; meanwhile adequate oxygen vacancies are also left in the bottom interface region so that R_{bot} is kept in the LRS. This may be contributed to the TiN_xO_y layer, which partly acts as an oxygen ion diffusion barrier,[18] so that oxygen vacancies can be maintained in the bottom interface region. As long as the configuration of R_{top}/R_{bot} is HRS/LRS (HRS0), the devices can present complementary resistive switching behaviours. The four-switching process, as depicted in Fig. 3, can be explained as follows: (1) with a voltage increasing under a negative bias, oxygen vacancies start to drift into the Pt/TiO_{2-x} top interface, and then R_{top} is switched to the LRS when $|V| > |V_{th,1}|$, after which the device is switched to the LRS ('ON' state) with R_{top}/R_{bot} in LRS/LRS (Fig. 5E). (2) With further increasing of the voltage under a negative bias, the bottom interface region is depleted of oxygen vacancies and switched to the HRS when $|V| > |V_{th,2}|$, then the device is turned into the '1' state with R_{top}/R_{bot} in LRS/HRS (Fig. 5F). (3) With a voltage increasing under a positive bias, oxygen vacancies from the top interface region start to fill the bottom interface region to rebuild a conductive path when $|V| > |V_{th,3}|$, then the device is switched to LRS ('ON' state) with R_{top}/R_{bot} in LRS/LRS (Fig. 5G). (4) With further increasing of the voltage under positive bias, the Pt/TiO_{2-x} top interface region is depleted of oxygen vacancies and switched to the HRS when $|V| > |V_{th,4}|$, then the device is switched to the '0' state with R_{top}/R_{bot} in HRS/LRS (Fig. 5H). During processes (1–4), oxygen ions in the TiN_xO_y layer may keep their immobility because the electric field is very small due to the high conductivity of this layer. Hence, the number of oxygen vacancies in the TiO_{2-x} layer might remain almost invariant during processes (1–4), ensuring the reversible complementary resistive switching behaviours.

On the basis of the above model, we can see that the stability of the complementary resistive switching of the device depends on the number of oxygen vacancies in the TiO_{2-x} layer. Thus the following two cases may happen: (Case 1) if oxygen vacancies are a deficiency, only conventional bipolar resistive switching could be observed (Fig. 2B). This situation could occur when a

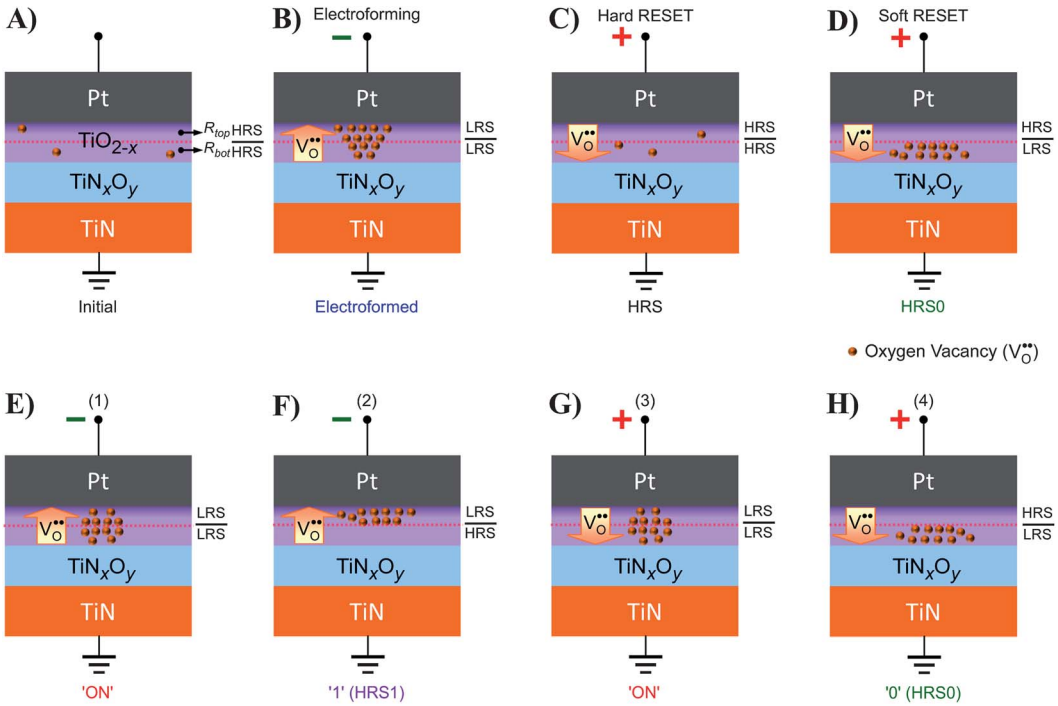

Fig. 5 Possible switching model for the complementary resistive switching behaviours in a Pt/TiO_{2-x}/TiN_xO_y/TiN device. Schematic illustration of oxygen vacancies redistributing in the memory cell. (A) Initial state of the device. (B–D) The electroforming, hard RESET and soft RESET processes, respectively. (E–H) The four-switching process (1–4) in fig. 3, respectively. The TiO_{2-x} nanolayer consists of two resistor regions in series, one at the top Pt/TiO_{2-x} interface (R_{top}) and the other at the bottom TiO_{2-x}/TiN_xO_y interface (R_{bot}). The red dashed line indicates the boundary of the two resistance regions. The migration direction of oxygen vacancies is indicated by the marked arrows.

hard RESET process is applied to result in both the top and bottom interfaces being in the HRS (Fig. 5C). (Case 2) If oxygen vacancies are in an overabundance, then the '0' or '1' state of the CRS cell may stay in an intermediate resistance state (IRS), the resistance of which is comparable to that of the 'ON' state. Fig. 6A shows such a case, where the '1' state is in an IRS. The reason could be attributed to oxygen vacancy formation at the TiO_{2-x}/TiN_xO_y bottom interface *via* eqn (1) under a negative bias.[20b] Hence, increasing the voltage under a negative bias could result in decreasing the resistance of the '1' state due to more oxygen vacancies being formed. In order to confirm this assumption, a large voltage range of (−1.2, 1.2) V was swept on the device (as shown in Fig. 6A), the resistance of the '1' state was further decreased as expected; while the resistance of the '0' state was increased slightly, which could be due to oxygen vacancy reduction at the bottom interface. In extreme conditions, the device may change into the CRS failed state for containing too many oxygen vacancies (in the LRS), for instance, through maloperation. Despite this, the device can be recovered to show CRS characteristics by a simple program, as shown in Fig. 6B: firstly, the failed device undergoes (i) a hard RESET process with a large positive bias (*e.g.*, 2 V) with R_{top}/R_{bot} in the HRS/HRS (as shown in Fig. 5C). Subsequently, the device undergoes (ii) an electroforming like process and (iii) a soft RESET process, similar to the programming of an as-prepared device. Finally, the failed device demonstrated CRS characteristics again (inset of Fig. 6B). The phenomenon observed in Fig. 6, especially the recovery of a CRS failed device reveals the reliability of our model. Besides, the recover capability of the device also guarantees a potential solution to extend the lifetime of RRAM.

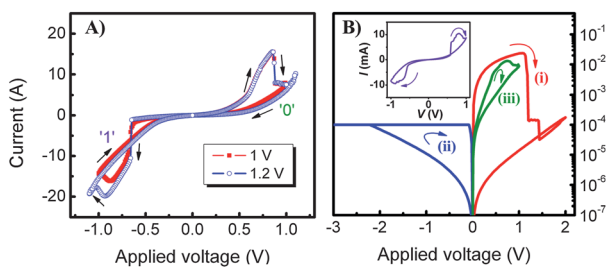

Fig. 6 (A) *I–V* curves of the '1' state of a Pt/TiO_{2-x}/TiN_xO_y/TiN device in the IRS on a linear scale. (B) Recover program of a CRS failed Pt/TiO_{2-x}/TiN_xO_y/TiN device (in theLRS). Inset: *I–V* curves of the device demonstrated CRS characteristics again after a recover program.

The recognition of complementary resistive switching behaviours is diverse. In brief, our model suggests that the rupture of the conducting path occurs at either the Pt/TiO_{2-x} interface or the TiO_{2-x}/TiN_xO_y interface, which lead to two storage states. Besides, over 100 complementary resistive switching cycles have been achieved from the non-optimised devices. Improvement of the CRS device would be focussed on reducing the operation current, enhancing the switching cycles and R_{HRS}/R_{LRS} ratio through further optimisations. Recently, Du *et al.* suggested that charge storage and release arise from the

trapping and de-trapping of oxygen molecular ions at the defect sites.[25] In the homo $TiO_x/TiO_y/TiO_x$ and hetero $TiO_x/TiON/TiO_x$ triple multilayer structures, the ruptures in the top and bottom TiO_x layers stands for two storage states.[8] The CRS was obtained in a higher voltage range in Ta_2O_5/TaO_x structure, while the conventional bipolar RS was obtained in a lower voltage range.[9] All the previous work,[8,9,25] and ours, suggest that the RS and modulating CRS are realized in a thin nanolayer in which the oxygen ions (or vacancies) are adjustable. Long term diffusion of the oxygen ions (or vacancies) hardly supports such a subtle modulation of oxygen ions (or vacancies), but might lead to a single-polarity RS mediated by the Schottky barrier.[26] Our results might provide a method to simplify the technological process to obtain CRS behaviours.

Conclusions

In summary, we have demonstrated complementary resistive switching behaviours in a TiO_{2-x} nanolayer-based RRAM with an operation voltage of 1 V. The memory structure of $TiO_{2-x}/TiN_xO_y/TiN$ was prepared by the one-step plasma oxidation of TiN films at room temperature. The real resistive switching occurs in the TiO_{2-x} nanolayer with a thickness of about 4 nm. Such complementary resistive switching behaviours can be interpreted by redistribution of oxygen vacancies between the Pt/TiO_{2-x} top interface and the TiO_{2-x}/TiN_xO_y bottom interface. The partly oxidised structure of the titanium oxynitride (TiN_xO_y) layer serves as both the oxygen reservoir and provider, and is essential for the bottom interface as it enables the resistive switching. In addition, the CRS failed cells can be recovered by a simple program, guaranteeing a potential solution to extend the life-time of RRAM. The titanium oxide nanolayer based RRAM with CRS characteristics provides a possible solution for future nanoscale crossbar memory arrays with cost-efficient feature.

Acknowledgements

This work was supported by National Basic Research Program of China (grant no. 2010CB832905), National Natural Science foundation of China (grant no. 51231004) and National Hi-tech (R&D) project of China (grant no. 2012AA03A706).

Notes and references

1 (*a*) J. J. Yang, M. D. Pickett, X. Li, D. A. A. Ohlberg, D. R. Stewart and R. S. Williams, *Nat. Nanotechnol.*, 2008, **3**, 429–433; (*b*) R. Waser, R. Dittmann, G. Staikov and K. Szot, *Adv. Mater.*, 2009, **21**, 2632–2663; (*c*) R. Waser and M. Aono, *Nat. Mater.*, 2007, **6**, 833–840; (*d*) Y. C. Yang, F. Pan, Q. Liu, M. Liu and F. Zeng, *Nano Lett.*, 2009, **9**, 1636–1643.

2 (*a*) S. H. Jo, K.-H. Kim and W. Lu, *Nano Lett.*, 2009, **9**, 870–874; (*b*) C. Kugeler, M. Meier, R. Rosezin, S. Gilles and R. Waser, *Solid-State Electron.*, 2009, **53**, 1287–1292.

3 (*a*) M.-J. Lee, Y. Park, B.-S. Kang, S.-E. Ahn, C. Lee, K. Kim, W. Xianyu, G. Stefanovich, J.-H. Lee, S.-J. Chung, Y.-H. Kim, C.-S. Lee, J.-B. Park, I.-G. Baek and I.-K. Yoo, *IEEE Int. Electron Devices Meet.*, 2007, 771–774; (*b*) M.-J. Lee, Y. Park, D.-S. Suh, E.-H. Lee, S. Seo, D.-C. Kim, R. Jung, B.-S. Kang, S.-E. Ahn, C. B. Lee, D. H. Seo, Y.-K. Cha, I.-K. Yoo, J.-S. Kim and B. H. Park, *Adv. Mater.*, 2007, **19**, 3919–3923; (*c*) M.-J. Lee, S. Seo, D.-C. Kim, S.-E. Ahn, D. H. Seo, I.-K. Yoo, I.-G. Baek, D.-S. Kim, I.-S. Byun, S.-H. Kim, I.-R. Hwang, J.-S. Kim, S.-H. Jeon and B. H. Park, *Adv. Mater.*, 2007, **19**, 73–76; (*d*) W. Y. Park, G. H. Kim, J. Y. Seok, K. M. Kim, S. J. Song, M. H. Lee and C. S. Hwang, *Nanotechnology*, 2010, **21**, 195201.

4 S. H. Jo and W. Lu, *Nano Lett.*, 2008, **8**, 392–397.

5 (*a*) M. Son, J. Lee, J. Park, J. Shin, G. Choi, S. Jung, W. Lee, S. Kim, S. Park and H. Hwang, *IEEE Electron Device Lett.*, 2011, **32**, 1579–1581; (*b*) J. J. Huang, Y. M. Tseng, C. W. Hsu and T. H. Hou, *IEEE Electron Device Lett.*, 2011, **32**, 1427–1429.

6 E. Linn, R. Rosezin, C. Kuegeler and R. Waser, *Nat. Mater.*, 2010, **9**, 403–406.

7 M.-J. Lee, C. B. Lee, D. Lee, S. R. Lee, M. Chang, J. H. Hur, Y.-B. Kim, C.-J. Kim, D. H. Seo, S. Seo, U. I. Chung, I.-K. Yoo and K. Kim, *Nat. Mater.*, 2011, **10**, 625–630.

8 Y. C. Bae, A. R. Lee, J. B. Lee, J. H. Koo, K. C. Kwon, J. G. Park, H. S. Im and J. P. Hong, *Adv. Funct. Mater.*, 2012, **22**, 709–716.

9 Y. C. Yang, P. Sheridan and W. Lu, *Appl. Phys. Lett.*, 2012, **100**, 203112.

10 B. J. Choi, D. S. Jeong, S. K. Kim, C. Rohde, S. Choi, J. H. Oh, H. J. Kim, C. S. Hwang, K. Szot, R. Waser, B. Reichenberg and S. Tiedke, *J. Appl. Phys.*, 2005, **98**, 033715.

11 F. Nardi, S. Balatti, S. Larentis and D. Ielmini, *IEEE Int. Electron Devices Meet.*, 2011, 709–712.

12 S. Kim and Y. K. Choi, *Appl. Phys. Lett.*, 2008, **92**, 223508.

13 (*a*) S. Facsko, T. Dekorsy, C. Koerdt, C. Trappe, H. Kurz, A. Vogt and H. L. Hartnagel, *Science*, 1999, **285**, 1551–1553; (*b*) R. Gago, L. Vazquez, R. Cuerno, M. Varela, C. Ballesteros and J. M. Albella, *Appl. Phys. Lett.*, 2001, **78**, 3316–3318.

14 R. Sanjines, H. Tang, H. Berger, F. Gozzo, G. Margaritondo and F. Levy, *J. Appl. Phys.*, 1994, **75**, 2945–2951.

15 (*a*) K. S. Robinson and P. M. A. Sherwood, *Surf. Interface Anal.*, 1984, **6**, 261–266; (*b*) I. Bertoti, M. Mohai, J. L. Sullivan and S. O. Saied, *Appl. Surf. Sci.*, 1995, **84**, 357–371.

16 J. M. Chappe, N. Martin, J. F. Pierson, G. Terwagne, J. Lintymer, J. Gavoille and J. Takadoum, *Appl. Surf. Sci.*, 2004, **225**, 29–38.

17 C. Yoshida, K. Tsunoda, H. Noshiro and Y. Sugiyama, *Appl. Phys. Lett.*, 2007, **91**, 223510.

18 J. S. Kwak, Y. H. Do, Y. C. Bae, H. S. Im, J. H. Yoo, M. G. Sung, Y. T. Hwang and J. P. Hong, *Appl. Phys. Lett.*, 2010, **96**, 223502.

19 T. Tamura, S. Ishibashi, K. Terakura and H. Weng, *Phys. Rev. B: Condens. Matter Mater. Phys.*, 2009, **80**, 195302.

20 (*a*) G. Chen, C. Song, C. Chen, S. Gao, F. Zeng and F. Pan, *Adv. Mater.*, 2012, **24**, 3515–3520; (*b*) D. S. Jeong, H. Schroeder and R. Waser, *Phys. Rev. B: Condens. Matter Mater. Phys.*, 2009, **79**, 195317; (*c*) H. Y. Jeong, J. Y. Lee and S. Y. Choi, *Adv. Funct. Mater.*, 2010, **20**, 3912–3917; (*d*)

D.-H. Kwon, K. M. Kim, J. H. Jang, J. M. Jeon, M. H. Lee, G. H. Kim, X.-S. Li, G.-S. Park, B. Lee, S. Han, M. Kim and C. S. Hwang, *Nat. Nanotechnol.*, 2010, **5**, 148–153.

21 (*a*) M. D. Pickett, D. B. Strukov, J. L. Borghetti, J. J. Yang, G. S. Snider, D. R. Stewart and R. S. Williams, *J. Appl. Phys.*, 2009, **106**, 074508; (*b*) J. P. Strachan, M. D. Pickett, J. J. Yang, S. Aloni, A. L. D. Kilcoyne, G. Medeiros-Ribeiro and R. S. Williams, *Adv. Mater.*, 2010, **22**, 3573–3577.

22 Y. C. Yang, X. X. Zhang, M. Gao, F. Zeng, W. Y. Zhou, S. S. Xie and F. Pan, *Nanoscale*, 2011, **3**, 1917–1921.

23 K. M. Kim, B. J. Choi, M. H. Lee, G. H. Kim, S. J. Song, J. Y. Seok, J. H. Yoon, S. Han and C. S. Hwang, *Nanotechnology*, 2011, **22**, 254010.

24 J. J. Yang, F. Miao, M. D. Pickett, D. A. A. Ohlberg, D. R. Stewart, C. N. Lau and R. S. Williams, *Nanotechnology*, 2009, **20**, 215201.

25 Y. M. Du, H. Pan, S. J. Wang, T. Wu, Y. P. Feng, J. S. Pan and A. T. S. Wee, *ACS Nano*, 2012, **6**, 2517–2523.

26 Y.-L. Chung, P. Y. Lai, Y.-C. Chen and J.-S. Chen, *ACS Appl. Mater. Interfaces*, 2011, **3**, 1918–1924.

